MULTISCALE ANALYSIS OF METAL / THERMOPLASTIC COMPOSITE INTERFACES USING ESI VPS

Sebastian Müller[1], Patrick de Luca[2] and Alain Tramecon[3]

[1] ESI Software Germany GmbH, Liebknechtstraße 33, 70565 Stuttgart, Germany,
sebastian.mueller@esi-group.com, https://www.esi-group.com
[2] ESI Group, 25 Rue Marcel Issartier, 33700 Mérignac, France,
Patrick.de.Luca@esi-group.com, https://www.esi-group.com
[3] ESI Group, 99 rue des Solets, Zone Silic 112, 94513 Rungis Cedex, France,
Alain.Tramecon@esi-group.com, https://www.esi-group.com

Keywords: Multiscale analysis, Material interfaces, Homogenization, Cohesive zone

ABSTRACT

The lack of maturity of composite crash simulation is still an issue in the introduction of composites in automotive mass production. This difficulty is amplified when one considers multi-material parts or assemblies. In the special case of laying thermoplastic composite tapes (using the ATL –Automatic Tape Laying - process) over a metallic surface, a key parameter is the texture of the metallic surface. The control of the texture involves the texturing process itself, the laying of the thermoplastic tapes and the mechanical performance of the final structure.
To this end, the present contribution deals with the numerical analysis of material interfaces between a metallic and a thermoplastic composite part. The goal is to develop an approach that allows for the simulation based characterization of laser structured material interfaces. The fundamental ideas of the virtual characterization process are given in Figure 1.

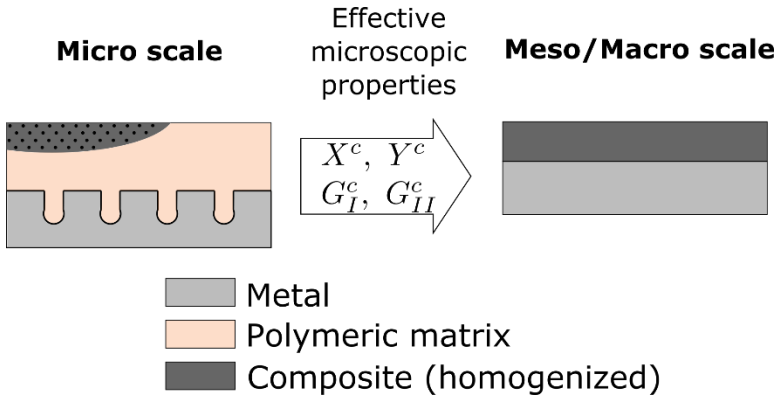

Figure 1: Virtual characterization of microscopic material interface features.

1 LASER STRUCTURED MATERIAL INTERFACES

The joinability of different materials is a key issue in the design of multi-material components. On the other hand the combination of certain materials in a single part allows for a significant optimization of lightweight structures towards performance and cost efficiency.
In the context of hybrid parts, consisting of metallic alloys and fiber reinforced polymers, the joint can be established utilizing the adhesive bond generated during the consolidation process of the composite. Since the generated adhesive strength is commonly significantly lower than the cohesive strength of the joint partners, the material interface is often the origin of component failure. An improvement of the adhesive properties can be achieved using chemical, electrical of mechanical mechanisms. The last mentioned category includes the generation of a mechanical interlock. On a microscopic scale this interlock can be generated through selective laser structuring of the metal surface (cf. Figure 2).

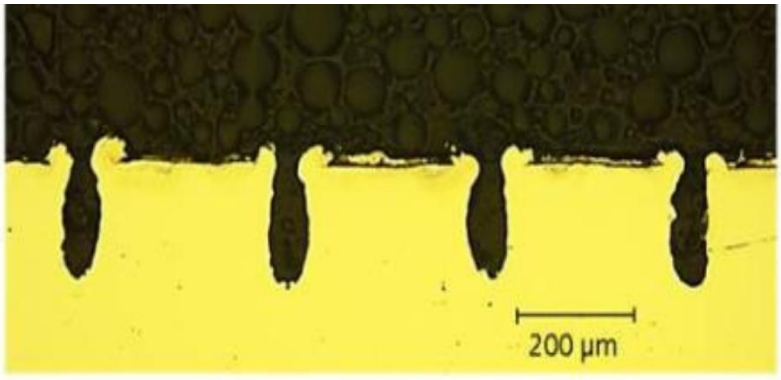

Figure 2: Micrograph of a laser structured composite-metal material interface.

2 MULTISCALE INTERFACE MODELLING

The evaluation of the performance of laser structured material interfaces usually requires extensive testing. In order to reduce the experimental effort, especially in an early design stage, a numerical modeling scheme has been developed. Following the works in [1,2], it is based on a multiscale analysis of the material interface that utilizes the contrast of length scale between the microscopic geometrical interface features and the macroscopic dimension of the hybrid structure. To this end, two scales are defined (cf. Figure 3). The characteristic length of the micro scale is of the magnitude as the size of the interface features generated by laser structuring, whereas the macro scale domain is of the same size as the hybrid part.

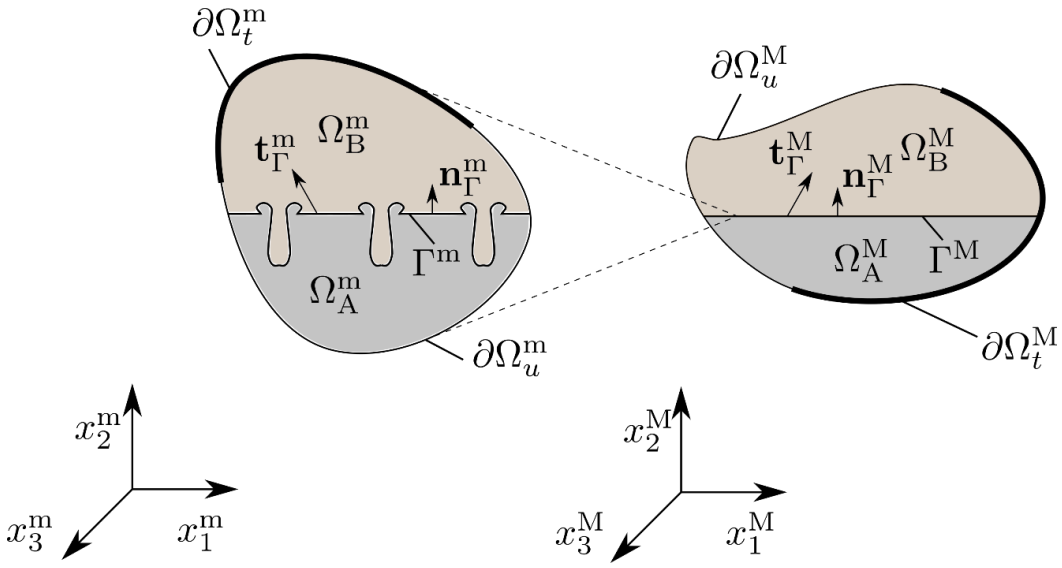

Figure 3: Micro-scale and Macro-scale domain definition.

The scale bridging between the micro- and the macro scale is accomplished using the well-known HILL averaging principle [3,4]. It relates the macroscopic virtual work density with the volume average of the total virtual work on the microscale.

3 MODEL GENERATION

Since the overall interface consists of a periodic repetition of unique geometric features, such as cavities, an RVE only consist of a representative section of the material interface (cf. Figure).

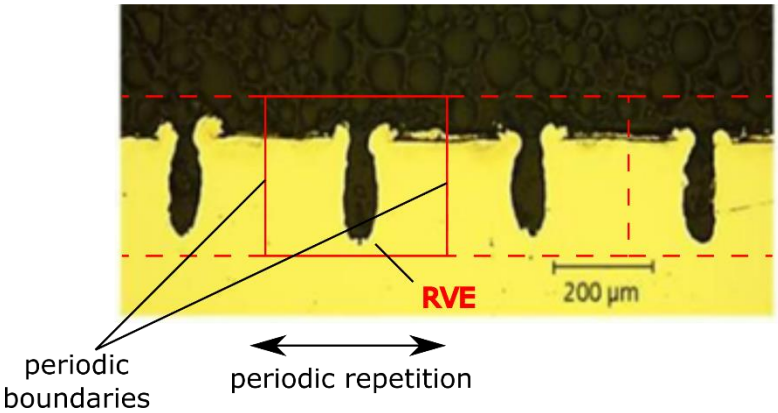

Figure 4: Definition of material interface RVE based on the periodic repetition of unique geometric interface features.

Depending on the complexity of the microscopic interface path, the generation of a finite element model can become very cumbersome. To this end, an automated modelling scheme has been developed. Starting from a homogeneous mesh, elements that are intersected by the material interface are automatically identified (cf. Figure 5).

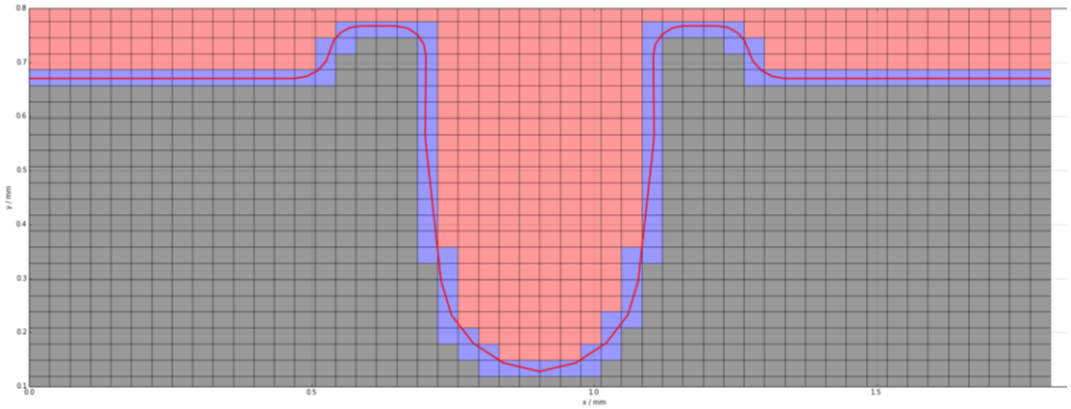

Figure 5: Micro-scale model generation with interface element identification (grey: metal elements, red: composite elements, blue: interface elements).

The geometrical interface path is further used to define an orthotropic frame for each interface element. To this end, the closest point of the interface path with respect to the element midpoint is identified. Once this is done the interface normal and tangential vector is calculated and used to define the local orthotropic frame of the element (cf. Figure 6).

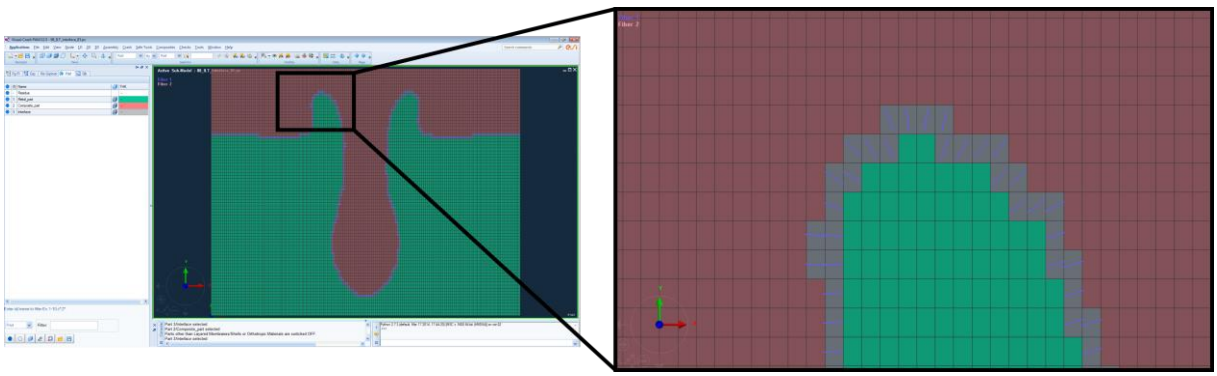

Figure 6: ESI VPS model of the microscopic laser structured interface with local interface normal direction definition.

The local orthotropic frame will be subsequently used to calculate the transferable traction over the material interface (cf. section 3).

3 CONSTITUTIVE RELATIONS

In order to properly analyze the effective interface properties based on a numerical model of the local interface structure, the essential effects of the material behavior need to be taken into account. This includes the modelling of all involved materials and the description of the interface behavior. While typical alloys can be assumed to remain linear elastic within the considered local loading exposure, inelastic material behavior need to be taken into account for the polymeric matrix and the material interface. This includes especially local damage mechanisms. While on a macroscopic scale pure cohesive damage between the two materials is considered and modeled, this failure divides into cohesive and adhesive damage on the microscale. To this end, the following sections will introduce a continuum damage model for the polymeric matrix and a cohesive damage model for the local interface.

3.1 Material interface model

On the microscopic scale the material interface is defined as the junction between the two material phases. In the present modelling approach this interface is represented through a set of finite elements that are interested by the material interface. Each of these elements has a unique local orthotropic frame nst, which has been derived from the local interface orientation (cf. Figure 7). This frame is subsequently used for the stress-strain calculation of the interface element.

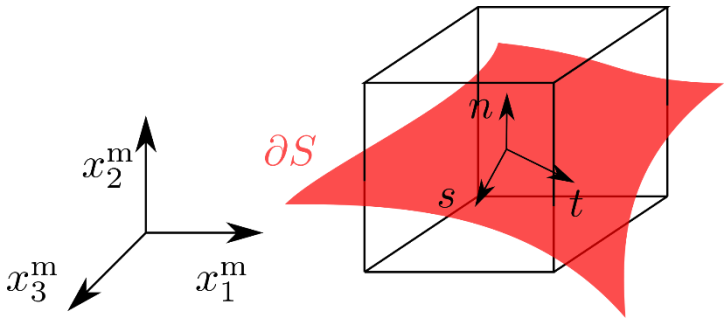

Figure 7: Local orthotropic frame nst defined by the orientation of the material interface ∂S.

In the present approach, the constitutive relation for the material interface is based on a hybrid continuum-cohesive material model initially introduced by Pineda&Waas [5] in the context of a shell progressive damage model. In the undamaged state, the interface material is assumed to behave linear elastic. The stress tensor is then defined as

$$\sigma_{ij} = C_{ijkl}\varepsilon_{kl}\,,\; C_{ijkl} = 2\mu\delta_{ik}\delta_{jl} + \lambda\delta_{ij}\delta_{kl} \tag{1}$$

with Lame parameters $\mu = \frac{E}{2(1+\nu)}$ and $\lambda = E/((1+\nu)(1-2\nu))$ and the Young's modulus E and the Poisson's ratio ν.

Damage initiation is assumed to take place once the interface tractions exceed the interface strength. In the present case this is detected using a quadratic failure criterion

$$\left(\frac{\langle \sigma_{nn} \rangle}{X_n}\right)^2 + \left(\frac{\sigma_{ns}}{Y_s}\right)^2 + \left(\frac{\sigma_{nt}}{Y_t}\right)^2 = 1 \tag{2}$$

with X_n, Y_s and Y_t the interface strength in normal and the two tangential directions, respectively. The Macaulay brackets prevent compressive normal tractions from influencing the damage initiation. After damage onset, the interface tractions are given by

$$\begin{aligned} \sigma_{nn} &= (1 - D^{\mathrm{CZ}}) K_{nn} \delta_{nn} \\ \sigma_{ns} &= (1 - D^{\mathrm{CZ}}) K_{ns} \delta_{ns} \\ \sigma_{nt} &= (1 - D^{\mathrm{CZ}}) K_{nt} \delta_{nt} \end{aligned} \tag{3}$$

with δ_{ni} the components of the interface separation vector and K_{ni} the interface secant stiffness at damage onset.
The separations are calculated from the local strain tensor

$$\begin{aligned} \delta_{nn} &= \varepsilon_{nn} l^{\mathrm{elem}}, \\ \delta_{ns} &= \gamma_{ns} l^{\mathrm{elem}}, \\ \delta_{nt} &= \gamma_{nt} l^{\mathrm{elem}}, \end{aligned} \tag{4}$$

using the characteristic length of the element l^{elem}. It can be seen that the degradation of all tractions is controlled by a unique scalar damage parameter D^{CZ}. The damage evolution is governed by a generalized form of the mixed mode cohesive damage model introduced by Camanho [6]. The damage driving force is an effective mixed mode separation defined as

$$\delta_m = \sqrt{\langle \delta_{nn} \rangle^2 + \delta_{ns}^2 + \delta_{nt}^2}. \tag{5}$$

The scalar damage parameter D^{CZ} is subsequently defined through a linear evolution function

$$D^{\mathrm{CZ}} = \frac{\delta_m^f (\delta_m^{max} - \delta_m^0)}{\delta_m (\delta_m^f - \delta_m^0)}. \tag{6}$$

with

$$\delta_m^{max} = \max\{\delta_m^{max}, \delta_m\} \tag{7}$$

the maximum effective mixed-mode separation reached during the loading history. The effective mixed mode separation at damage onset δ_m^0 and δ_m^f at total decohesion follow directly from the mixed mode initiation criteria, the definition of the effective mixed mode separation and the mixed mode fracture criterion

$$\left(\frac{G_I}{G_{IC}}\right) + \left(\frac{G_{IIs}}{G_{IICs}}\right) + \left(\frac{G_{IIt}}{G_{IICt}}\right) = 1 \tag{8}$$

with G_{IC} the mode I and G_{IICs} / G_{IICt} the mode II fracture toughness.

3.1 Material interface model

A nonlinear elastic material behavior is assumed for the polymeric matrix phase. The model is obtained as a derivative of the model presented by Müller et al. [7]. The multiaxial stress-strain relation is given by

$$\sigma_{ij} = \frac{2G}{1+\alpha_G\|e_{kl}\|}e_{ij} + \frac{2K}{1+\alpha_K|\varepsilon_{mm}|}\varepsilon_{mm}\delta_{ij} \tag{9}$$

with δ_{ij} the Kronecker delta, e_{ij} the deviatoric strain tensor, ε_{mm} the volumetric strain. The shear modulus G and the compression modulus K as well as the nonlinearity parameters α_G and α_K are defined as function of the uniaxial material parameters E, ν, α

$$G = \frac{E}{2(1+\nu)}, \qquad K = \frac{E}{3(1-2\nu)}, \tag{10}$$
$$\alpha_G = \sqrt{\frac{3}{2}}\frac{\alpha}{(1+\nu)}, \qquad \alpha_K = \frac{\alpha}{(1-2\nu)}.$$

They can be efficiently identified from uniaxial tensile tests (cf. Kästner et al. [8]).

The continuum damage model for the polymer is further defined to allow for a local degradation of the material stiffness. The damage initiation is defined by the Christensen failure criterion with tensile and compressive strength T and C

$$\left(\frac{1}{T}-\frac{1}{C}\right)(\sigma_{11}+\sigma_{22}+\sigma_{33}) + \frac{1}{2TC}[(\sigma_{11}-\sigma_{22})^2+(\sigma_{22}-\sigma_{33})^2+(\sigma_{33}-\sigma_{11})^2] \leq 1. \tag{11}$$

Once damage initiation has been detected the stress is degraded based on the effective stress principle by the scalar damage variable D^{CDM}.

$$\sigma_{ij} = (1-D^{\mathrm{CDM}})\hat{\sigma}_{ij}. \tag{12}$$

An equivalent displacement is defined based on an equivalent strain proposal given by de Vree et al. [9]

$$\delta_v = l^{\mathrm{elem}}\left(k_1 I_1 + \sqrt{(k_1 I_1)^2 + k_2 J_2}\right) \tag{13}$$

with I_1 and J_2 the first and second invariant of the strain tensor as well as the coefficients

$$k_1 = \frac{\gamma-1}{2\gamma(1-2\nu)} \text{ and } \mathrm{k}_2 = \frac{3}{\gamma(1+\nu)^2}. \tag{14}$$

Here γ is the ratio of the compressive strength to tensile strength. A linear damage evolution law is defined

$$D^{\mathrm{CDM}} = \frac{\delta_v^f(\delta_v^{max}-\delta_v^0)}{\delta_v^{max}(\delta_v^f-\delta_v^0)} \tag{15}$$

Using δ_v^0 and δ_v^f the equivalent displacement at damage onset and total failure, respectively. The later one is directly related to the fracture energy G_f and the von Mises stress at damage initiation σ_{vM}^0

$$\delta_v^f = \frac{2G_f}{\sigma_{vM}^0}. \tag{16}$$

4 SIMULATION

The developed multi-scale modelling framework for laser structured material interfaces is subsequently applied to a set of evaluation problems. Therefor it has been implemented in the commercial FEM package ESI Virtual Performance Solution (VPS).

The interface geometries analyzed in the present contribution have been provided from the Fraunhofer Institute for Laser Technology ILT in Aachen, Germany. Three different interface feature geometries have been created based on experimental observations. They are linked to different intensities of the laser structuring. Sketches of the three types are shown in Figure 8.

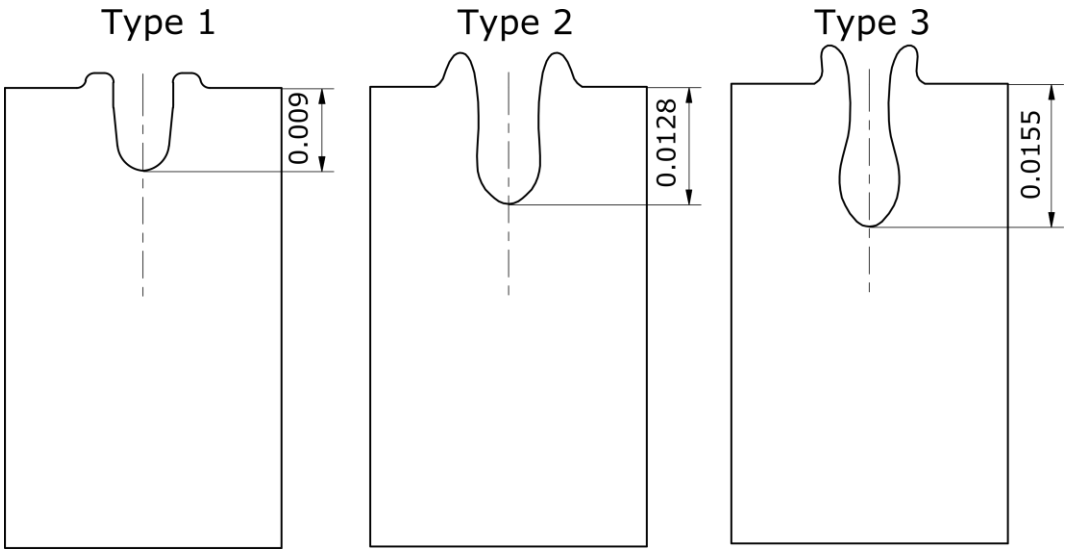

Figure 8: Three different idealized geometrical interface features generated by Fraunhofer Institute for Laser Technology ILT in Aachen, Germany.

The corresponding VPS models generated by the previously introduced voxel approach can be seen in Figure 9. A constant element length of 2e-4 mm has been used throughout all simulations.

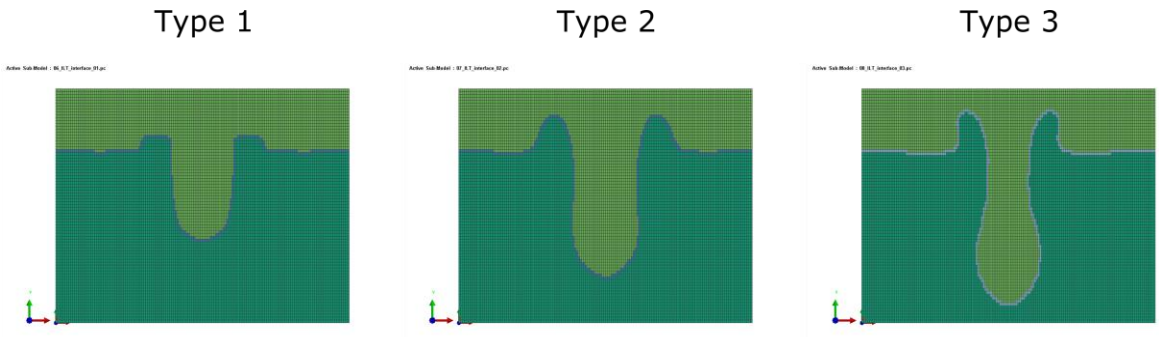

Figure 9: VPS models of three types of interface textures.

Since calibration data for the different constitutive relations is yet not available, empirical values have

been used instead (cf. Table 1).

Material	Parameter		Value
Metal - AHSS	E	[GPa]	222
	ν	–	0.284
Polymer – PA66	E	[GPa]	1.7
	ν	–	0.3
	T	[GPa]	0.083
	C	[GPa]	0.087
	G_f	[GPa·mm]	0.002
Interface	E	[GPa]	1.7
	ν	–	0.3
	X_n	[GPa]	0.01
	Y_s	[GPa]	0.01
	Y_t	[GPa]	0.01
	G_{IC}	[GPa·mm]	9e-5
	G_{IICs}	[GPa·mm]	2e-4
	G_{IICt}	[GPa·mm]	2e-4

Table 1: Empirical material parameters used for the demonstration problems.

The three interface types have been analyzed for different loading conditions. To this end, a monotonic increasing displacement has been applied to the nodes on the upper boundary surface of the model, while the bottom nodes where clamped. The loading mode (e.g. mode I, II and mixed mode) is defined by the load angle α. Note that periodic displacement boundary conditions have been applied to the left and right boundary surface to account for the periodicity of the structure (cf. Figure 10).

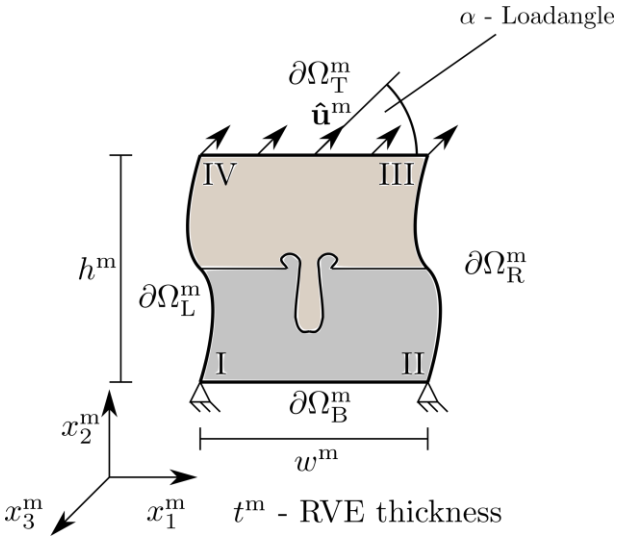

Figure 10: Interface RVE model with boundary surface definition and boundary conditions.

Three different loading angles have been analyzed: (I) α=90° - Mode I, (II) α=45° - Mixed Mode, (III) α=0° - Mode II. The resulting effective stress- displacement curves are compared in Figure 11.

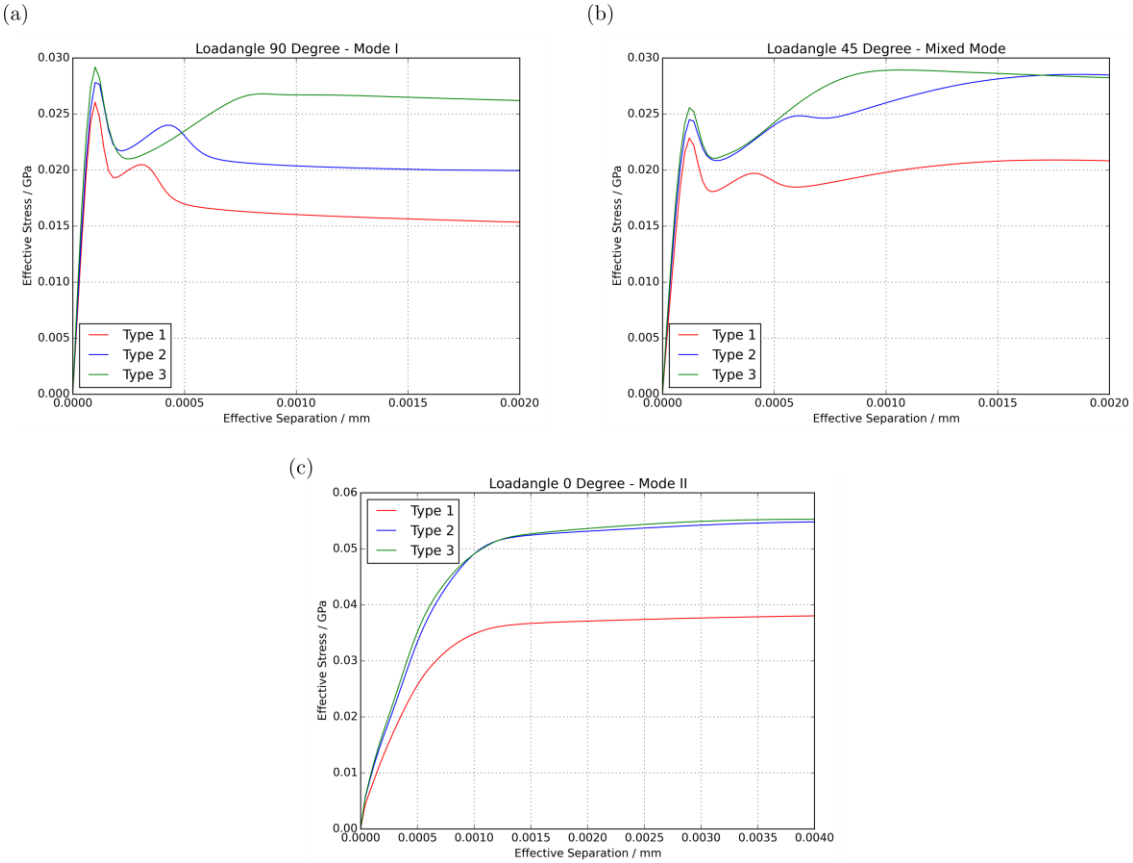

Figure 11: Effective stress-displacement curves for the three interface models shown in Figure 9: (a) pure mode I loading, (b) mixed mode loading and (c) pure mode II loading.

It can be seen that the effective strength of the interface is significantly influenced by the geometrical structure. The predicted strength values (peak of the stress-displacement curves) are significantly increased compared with the original strength of the interface in normal and tangential direction (0.01 GPa, cf. Table 1). While the first peak is always due to interface damage, the second peak observed for mode I and mixed mode is caused by failure of the polymeric matrix material. An overview of the damage pattern at the end of the simulation is shown in Figure 12 for the interface and matrix damage of all three interface types under the three loading conditions. While mode I loading causes only interface damage for type 1 and 2, the mechanical interlook of type 3 causes damage in the matrix phase, too. For all interface types, the metal bumbs generated by the laser structuring process are the origin for damage within the matrix phase.

5 CONCLUSIONS

The present contribution introduces a novel approach to characterize the mechanical performance of laser structured material interfaces between a metal and a composite part. To this end, a multiscale framework is applied introducing a micro and a macro scale. The scale bridging is accomplished using the well-known HILL averaging principle. An automated model generation scheme has been developed that transfers the geometrical interface data into a voxel type FE model. The characteristic damage phenomena on the micro scale, namely interface and matrix damage, are captured through specific constitutive models. Both the model generation and the material model implementation has been accomplished using the commercial FEA package ESI Virtual Performance Solution (VPS). A proof of concept has been made by simulating three different interface geometries under three different loading conditions. It has been shown that the microstructure has a strong influence on the effective mechanical performance and that the overall microscopic damage is a combination of adhesive interface and cohesive matrix damage. In the future the modeling approach will be systematically parametrized and validated using extensive mechanical testing.

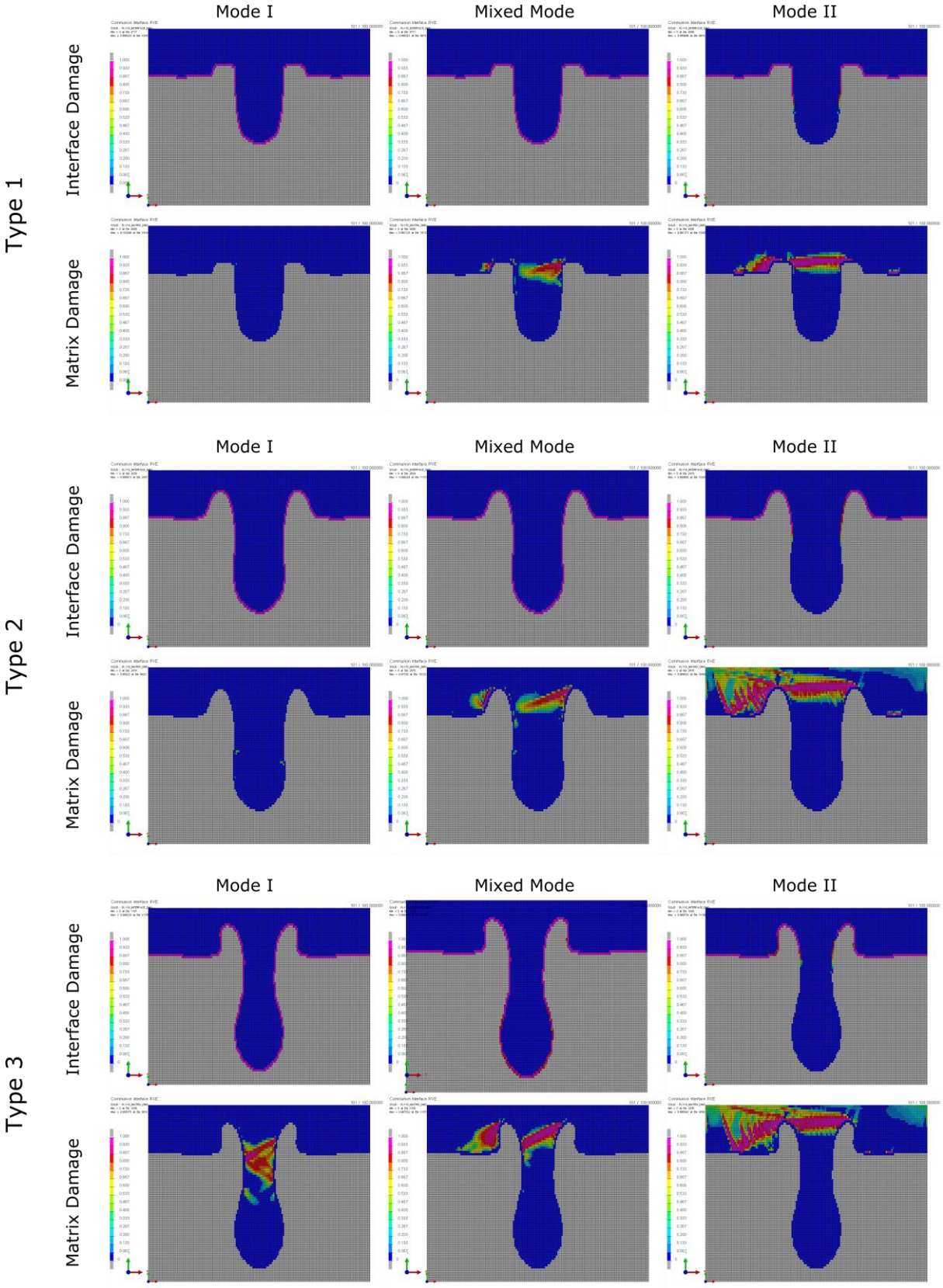

Figure 12: Damage pattern at the end of the simulations for three interface types (1/2/3) and three loading conditions (mode I, mixed mode, mode II).

ACKNOWLEDGEMENTS

This work is under the framework of EU Project Communion. This project has received funding from the European Union's Horizon 2020 research and innovation program under grant agreement No 680567. The Authors thankfully acknowledge the financial support as well as the all industrial, academic and research partners contributing assistance to the presented work.

REFERENCES

[1] M. Cid Alfaro, A. Suiker, C. Verhoosel, R. de Borst, 2010. Numerical homogenization of cracking processes in thin fibre-epoxy layers. In: European Journal of Mechanics - A/Solids 29 (2), pp. 119–131.

[2] F. Hirsch, M. Kästner, 2016. Microscale simulation of adhesive and cohesive failure in rough interfaces, In: Engineering Fracture Mechanics - accepted.

[3] R. Hill, 1963. Elastic Properties of Reinforced Solids: Some Theoretical Principles. In: J.Mech. Phys. Solids 11, pp. 357–372.

[4] R. Hill, 1972. On constitutive macro-variables for heterogeneous solids at finite strain. In: Proc. R. Soc. Lond. A., pp. 131–147.

[5] E. J. Pineda, A. M. Waas, 2013. Numerical implementation of a multiple-ISV thermodynamically-based work potential theory for modeling progressive damage and failure in fiber-reinforced laminates. In: International Journal of Fracture, pp. 93-122.

[6] P. P. Camanho, C. G. Dávila, M. F. De Moura, 2003. Numerical Simulation of Mixed-mode Progressive Delamination in Composite Materials. In: Journal of Composite Materials, Vol. 37, pp. 1415-1438.

[7] S. Müller, M. Kästner, V. Ulbricht, 2011, A nonlinear fractional viscoelastic material model for polymers, Computational Materials Science, Vol. 50, Issue 10, pp. 2938-2949.

[8] M. Kästner, M. Obst, J. Brummund, K. Thielsch, V. Ulbricht, 2012. Inelastic material behavior of polymers – Experimental characterization, formulation and implementation of a material model. In: Mechanics of Materials, Vol. 52, pp. 40-57.

[9] J. de Vree, W. Brekelmans, A. Van, 1995, Comparison of nonlocal approaches in continuum damage mechanics. In: Computers and Structures, Vol. 55, pp. 581-588.